On the importance of tunica intima in the aging aorta: a three-layered in silico model for computing wall stresses in abdominal aortic aneurysms

Mario de Lucio [a], Marcos Fernández García[b], Jacobo Díaz García[c], Luis Esteban Romera Rodríguez[c], Francisco Álvarez Marcos[d]

[a]School of Mechanical Engineering, Purdue University, 585 Purdue Mall, West Lafayette, IN 47907, USA;
[b]Structural Impact Laboratory (SIMLab) and Centre for Advanced Structural Analysis (CASA), Department of Structural Engineering, Norwegian University of Science and Technology (NTNU), NO-7491 Trondheim, Norway;
[c]Structural Mechanics Group, School of Civil Engineering, Universidade da Coruña, Campus de Elviña s/n, 15071, A Coruña, Spain;
[d]Angiology and Vascular Surgery Department, Asturias University Central Hospital (HUCA), Oviedo, Spain

ARTICLE HISTORY
Compiled September 21, 2020

ABSTRACT
Layer-specific experimental data for human aortic tissue suggest that, in aged arteries and arteries with non-atherosclerotic intimal thickening, the innermost layer of the aorta increases significantly its stiffness and thickness, becoming load-bearing. However, there are very few computational studies of abdominal aortic aneurysms (AAAs) that take into account the mechanical contribution of the three layers that comprise the aneurysmal tissue. In this paper, a three-layered finite element model is proposed from the simplest uniaxial stress state to geometrically parametrized models of AAAs with different asymmetry values. Comparisons are made between a three-layered artery wall and a mono-layered intact artery, which represents the complex behavior of the aggregate adventitia-media-intima in a single layer with averaged mechanical properties. Likewise, the response of our idealized geometries is compared with similar experimental and numerical models. Finally, the mechanical contributions of adventitia, media and intima are analyzed for the three-layered aneurysms through the evaluation of the mean stress absorption percentage. Results show the relevance and necessity of considering the inclusion of tunica intima in multi-layered models of AAAs for getting accurate results in terms of peak wall stresses and displacements.

KEYWORDS
Arterial wall mechanics ; Abdominal aortic aneurysm; Tunica intima

1. Introduction

An abdominal aortic aneurysm (AAA) is a balloon-like, localized enlargement of the aorta that bulges out beyond the normal diameter of the blood vessel. AAAs affect about 3% of the world population over the age of 50 (LeFevre 2014). Associated risk

Corresponding author: Mario de Lucio. Email: mdeluci@purdue.edu

factors are mostly lifestyle-related (smoking, dyslipidemia, high blood pressure), although a heritable component can also play a role. They usually remain asymptomatic until rupture, which can lead to life-threatening internal bleeding with an in-hospital mortality of about 40% and a pre-hospitalization overall mortality of 80% (Kühnl et al. 2017). Repair of an AAA may be done either by open surgery or endovascular aneurysm repair (EVAR). Open repair, as any surgical procedure, may associate with a non-negligible rate of complications such as bleeding during or after surgery, myocardial infarction, respiratory impairment or graft infection. On the other hand, EVAR is a minimally invasive technique that only requires small incisions in the groin, but requires a more strict postoperative surveillance over time.

The current approach to assess the risk of rupture and to determine whether the patient should undergo surgical repair or not is a dimensional criterion based on the maximum diameter of the lesion (aortic size). If the maximum diameter increases more than 0.5–1 cm in one year, or if it reaches 5.0 cm in women or 5.5 cm in men, surgical repair will be necessary (Lederle et al. 2002; Hans et al. 2005; Grootenboer et al. 2009). Nonetheless, about 13% of AAAs with an aortic size of less than 5 cm rupture, whereas 54% of those over 7 cm may not rupture over long periods. Therefore, a more reliable parameter is needed for the assessment of the risk of AAA rupture. Peak wall stresses are suggested by many studies (Rodríguez et al. 2009; Vorp et al. 1998; Raghavan et al. 1996) as a more suitable parameter than the current diameter criterion. However, peak wall stresses cannot be measured in complex geometries just by applying simple analytic techniques, hence, numerical modeling must be used. In this respect, the finite element analysis provides a convenient numerical tool to calculate approximate wall stresses that facilitates the evaluation of the rupture potential of AAAs.

From the biomechanical point of view, the aortic wall consist of three layers: adventitia, the outermost layer; tunica media, which is the medial layer, and tunica intima, which is the innermost layer. In young human arteries and arteries of laboratory animals, only the adventitia and media are load-bearing layers and the intima is just a thin layer made up mostly of endothelial cells. However, in aged arteries, the intima attains a significant thickness and the three layers become load-bearing. This is caused by diffuse intimal thickening or intimal hyperplasia, which is considered to be the precursor of atherosclerosis and produces the collagenization of the intima (Movat et al. 1958). Some studies explain the thickening as a compensatory response to the wall shear reduction, so that the artery decreases the luminal diameter in response to a reduced blood flow in order to restore shear stress (Glagov and Zarins 1989). Nevertheless, there are very few computational studies of AAAs that take into account the mechanical contribution of the intima as an individual layer with its own mechanical properties.

Many researchers have extensively studied the layer-specific mechanical properties of human thoracic and abdominal aortas. Weisbecker et al. (2012) tested 14 thoracic aortas and 9 abdominal aortas from patients aged between 55 to 77 years with acute non-atherosclerotic intimal thickening, obtaining the material parameters for each layer. Kobielarz et al. (2017) analyzed 27 thoracic aortas from young patients with a mean age of 26 years and early atherosclerotic lesions, concluding that the intima is load-bearing. Amabili et al. (2019) characterized the layer-specific hyperelastic and viscoelastic behaviour of 12 healthy descending thoracic aortas from patients with an average age of 49 years. Akyildiz et al. (2014) studied the mechanical properties of the intimal layer in the presence of atherosclerotic plaques, showing a great dispersion in the tensile and compressive properties of the plaque. Barrett et al. (2019) made a review on the imaging techniques, the experimental tests and the computational methods used to obtain calcified plaque tissue properties, concluding that it is necessary to carry out experimental tests down in scale, towards micron and submicron scales, to understand the calcified plaque mechanical behaviour. In the case of aortic aneurysms, one of the first works to characterize the mechanical properties of each layer was performed by Sokolis et al. (2012), studying layer heterogeneity in 8 ascending thoracic aortic aneurysms from patients aged between 60 to 80 years. Sassani et al. (2015) determined layer dependent tissue properties in abdominal aortic aneurysms from 15 patients aged between 58 and 85 years. Deveja et al. (2018) analyzed the mechanical properties of each layer in thoracic aortic aneurysms and non-aneurysmal aortas from 17 patients.

Even from the development of multi-layer constitutive relations for arterial walls by Gasser et al. (2006), and the obtaining of the layer-specific material parameters by several researchers, the intima has been excluded from numerical studies due to its small thickness in young arteries (Alastrué et al. 2007). Prior studies have performed isotropic finite element simulations considering elastic or hyperelastic constitutive laws in mono-layered arterial walls, like Scotti et al. (2005) and Raghavan and Vorp (2000). Other authors carried out more advanced computational models implementing the anisotropy of the arterial wall in patient-specific geometries like Xenos et al. (2010) for a mono-layered AAA wall, Rodríguez et al. (2008) for different idealized mono-layered AAAs, or Alastrué et al. (2007) for a two-layered iliac artery, in which only adventitia and media were taken into account. Further research on hyperelastic constitutive laws also include the numerical implementation of residual stresses, like Ahamed et al. (2016) for evaluating wall stresses using mono-layered patient-specific geometries, or Labrosse et al. (2013), where residual stresses are obtained by experimental testing on pressurized ascending, thoracic and abdominal cylindrical samples. However, none of them consider the increase in stiffening and thickness of the innermost layer of the aorta.

Regarding experimental studies on residual stresses and their spatial distribution in the aortic wall, the next contributions could be highlighted. Sokolis et al. (2017) performed a detailed experimental identification of the spatial distribution of circumferential residual strains in human aorta considering age and gender; they also studied the regional and interlayer distribution of residual deformations and opening angles in porcine aortas in (Sokolis 2019). Amabili et al. (2019) measured opening angles in ascending human aortas to identify the circumferential residual stresses and axial stretches. Finally, among the few studies of residual strains in aneurysms, the work by Sokolis (2015) on ascending thoracic arteries, considering the variation of residual deformations in the different aortic layers; and the work by Sassani et al. (2015) obtaining layer dependent residual stretch measurements in abdominal aortic aneurysms, must be featured.

The first three-layered models assumed an isotropic linear elastic response for all the layers, like Gao et al. (2006, 2008) for three-layered aneurysmal and non-aneurysmal aortic archs, where the Young's modulus of the medial layer was assumed to be three times larger than that of the intimal and adventitial layer. Gao et al. also peformed FSI analyses on two dimensional (2D) axisymmetric geometric models of stented three-layered aneurysms (Gao et al. 2013). Simsek and Kwon (2015) and Gholipour et al. (2018) evaluated the rupture potential of three-layered idealized aneurysmal and non-aneurysmal geometries assuming different hyperelastic isotropic material properties for each layer. Recent studies analyzed the inclusion of residual stresses in three-layered aneurysms, like Pierce et al. (2015) for a patient-specific geometry. Other researchers like Strbac et al. (2017) even studied how to improve the finite element codes for computing faster, and more accurate solutions in three-layered patient-specific geometries.

Nonetheless, the structural role played by tunica intima during the development of atherosclerosis, and its through-the-thickness stress distribution has not been clarified yet.

This work proposes a three-layered model that allows to study the influence of intimal thickening from a mechanical point of view on different parametrized geometrical models of AAAs. The calibration of the material model, which is considered hyperelastic anisotropic, is done through finite element simulations of uniaxial tests of aorta strips cut in the circumferential and axial direction, and the inflation of plane strain aorta rings subjected to systolic blood pressure. Then, peak wall stresses and displacements are computed in three different idealized AAA geometries considering a three-layered wall, in which each layer is modeled separately in a continumm mesh using different material parameters, and an intact monolayered human aorta wall. As loading conditions, we apply a static internal pressure of 16 kPa (120 mmHg) to simulate the luminal pressure at the end-systolic state. No residual stresses are considered. Additionally, comparisons between the three-layered and the intact wall are made, as well as between different material models (elastic and hyperelastic isotropic) from other studies. Finally the stiffness of each layer that make up the aneurysmal tissue is evaluated and compared through its mean stress absorption percentage.

2. Methods

2.1. Constitutive behavior of arterial tissue

Constitutive modeling of arterial tissue has undergone a significative evolution over the past decade. Early-modeled aneurysmal tissue was characterized as a single layer linear elastic material (Martino et al. 2001; Li and Kleinstreuer 2007; Georgakarakos et al. 2010; Wang and Li 2011). As a consequence of the uniaxial testing of aortic tissue specimens carried out by Raghavan et al. (2000), the nonlinear elastic behaviour is incorporated in material models, where the mechanical behavior of the arterial wall was, for the first time, modeled as hyperelastic, with a constitutive law based on a simplified criterion derived from the Mooney-Rivlin strain energy function. Thereafter, the vast majority of the computational studies of fully developed aneurysms assumed isotropy (Wang et al. 2002; Chandra et al. 2013; Li et al. 2008; Maier et al. 2010). A high degree of anisotropy was subsequently noticed by Geest et al. (2006) after performing biaxial testing to characterize the mechanical properties of aortic tissue in the longitudinal and circumferential direction. Then, the obtained experimental data would be fitted to a four parameter exponential strain function proposed by Vito and Hickey (1980). Later on, the understanding of the arterial histology by means of extensive experimental data has led to new and more accurate constitutive models that make it possible to analyze the multi-layered nature of the arterial wall as an anisotropic fiber-reinforced material (Holzapfel et al. 2000). The aforementioned continuum approach was considered in this study by means of the constitutive model developed by Holzapfel et al. (2000) and Gasser et al. (2006). This model asserts that each artery layer may be understood as a composite reinforced material constituted by two families of collagen fibers embedded in a soft incompressible matrix, which is mostly made up of elastin. The collagen fibers are arranged in spirals and symmetrically oriented with respect to the circumferential direction. The strain energy function used to model each layer of the artery wall is given by

$$\Psi = \Psi_{\text{iso}} + \Psi_{\text{aniso}}. \tag{1}$$

Ψ can be divided in an isotropic part, Ψ_{iso}, which represents the energy stored in the non-collagenous soft matrix, and anisotropic part, Ψ_{aniso}, which provides the energy stored in the collagen fibers

$$\Psi_{\text{iso}} = \frac{\mu}{2}\left(\bar{I}_1 - 3\right) \tag{2}$$

$$\Psi_{\text{aniso}} = \frac{k_1}{2k_2}\sum_{i=1}^{N=2}\left[\exp\left(k_2\bar{E}_i^2\right) - 1\right]. \tag{3}$$

$\bar{E}_i$, which stands for the Green-Lagrange strain-like quantity, can be expressed as

$$\bar{E}_i = \kappa\bar{I}_1 + (1-3\kappa)\left(\bar{I}_{4i} - 1\right) \tag{4}$$

where

$$\bar{I}_{4i} = \mathbf{a}_{0i}\otimes\mathbf{a}_{0i} : \bar{\mathbf{C}}. \tag{5}$$

The non-collagenous soft matrix is modeled as an incompressible isotropic neo-Hookean material, with $\mu > 0$ as the shear modulus in the undeformed configuration, and $\bar{I}_1$ as the first strain invariant of a modified right Cauchy-Green tensor, $\bar{\mathbf{C}} = \bar{\mathbf{F}}^{\mathbf{T}}\bar{\mathbf{F}}$. $\bar{\mathbf{F}}$ represents the isochoric part of the deformation gradient and comes from a multiplicative decomposition of the deformation gradient $\mathbf{F} = \left(J^{\frac{1}{3}}\mathbf{I}\right)\bar{\mathbf{F}}$, where $J^{\frac{1}{3}}$ and $\bar{\mathbf{F}}$ represent the volumetric and isochoric part of the deformation gradient, respectively, and $\mathbf{I}$ is a second-order unit tensor. In equation (3) the strain energy stored in the collagen fibers is defined as an exponential function, where N is the number of fiber families of each layer. In accordance with Schriefl et al. (2012), a two-fiber family is considered for all the layers in this study. $k_1 > 0$ is a stress-like parameter, while $k_2 > 0$ is a dimensionless parameter, and both are determined from mechanical tests of the tissue. $\bar{E}_i$ represents the strain in the direction defined by the mean orientation of each fiber family, which is in turn denoted by the vector $\mathbf{a}_{0i}$. The parameter $\kappa \in [0, 1/3]$ is also unitless and describes the level of dispersion of the fiber directions. According to the value of κ, collagen fibers may be perfectly aligned ($\kappa = 0$), which means that there is no dispersion, or randomly distributed ($\kappa = 1/3$), which corresponds with a spherical distribution of the density function and the material becomes isotropic. κ and $\mathbf{a}_{0i}$ are determined from histological data. Finally, $\bar{I}_{4i}$ is the pseudo-invariant of $\bar{\mathbf{C}}$.

The material model presented above was used in all our simulations. It is based on experimental tests and histological analysis performed on non-aneurysmal aortas considering two families of collagen fibers. Other authors like Gasser et al. (2012) and Sassani et al. (2015), have made improvements to this model by identifying the spatial organization of the collagen fiber network. In these works, the spatial distribution of collagen in each layer of the aortic wall, which determines its strength and stiffness, is reproduced more precisely using three families of collagen fibers instead of two, one circumferential and two diagonals, allowing a better characterization of the risk of aortic rupture.

2.2. Finite element modeling

The simulations presented in this article were conducted by using the FEM commercial software Abaqus/Standard 6.14, in which the constitutive model explained previously is built-in (201 2014b). To check the viability of the proposed three-layered model, different geometries were considered, and in all of them we used the thicknesses and average properties of each layer obtained experimentally by Weisbecker et al. (2012) for the abdominal aorta. From the simplest to the most complex one, we developed finite element models of uniaxial tests performed on rectangular aorta strips cut in the axial and circumferential direction, human aorta plane strain rings, and finally three different parametrized geometric aneurysms with intimal thickening. Residual stresses are not included in the finite element models developed.

In the three types of finite element models developed, experimental mechanical properties of non-aneurysmal abdominal aortic tissues are used, so that all models share the same properties and the results could be comparable.

3. Finite element models of uniaxial test of aorta strips

Based on the work developed in Gasser et al. (2006), finite element computations of uniaxial tension tests were performed on rectangular intact and layer-separated aorta strips with non-athersclerotic intimal thickening cut in the axial and circumferential direction. The specimens are loaded in the longitudinal direction with a force F that produces an elongation δ and are assumed to be stress free in the undeformed configuration. The definition of axial and circumferential specimens as well as the model configuration are illustrated schematically in Figure 1.

The referential dimensions of the strips were 20 mm for the length, 6 mm for the width and a total thickness of 2.69 mm. In the three-layered separated strips, the thickness of the different layers that comprise the tissue are: 0.68 mm for the intima, 0.94 mm for the media and 1.07 mm for the adventitia. The in-plane dimensions are based on the ones provided in the Abaqus Benchmarks Guide (201 2014a), where a rectangular 10 x 3 x 0.5 mm adventitial strip is analyzed under uniaxial tension. Since we had a maximum thickness of 1.07 mm and we wanted to keep a similar in-plane aspect ratio not to distort the results, the final dimensions of our strips had to be bigger by a factor of two compared to the benchmark model. Regarding the thicknesses, they are in accordance with the median thicknesses of the intima, media and adventitia determined by Weisbecker et al. (2012). The different material constants as well as the orientations of the two families of fibers considered for the layer-separated and the intact artery wall, which considers the aggregate adventitia-media-intima in a single layer with averaged mechanical properties, are summarized in Table 1.

Exploiting the symmetry of the problem, only one half of the geometry was modeled. To model the incompressible deformation of the arterial tissue with sufficient precision, a total of 12,000 eight node linear solid hybrid elements (C3D8H) were used for the adventitia, 12,100 for the media and 36,000 for the intima, with a minimum of three elements through-the-thickness, whereas 60,000 elements were required for the intact layer models. Regarding the type of element used, it is important to consider the

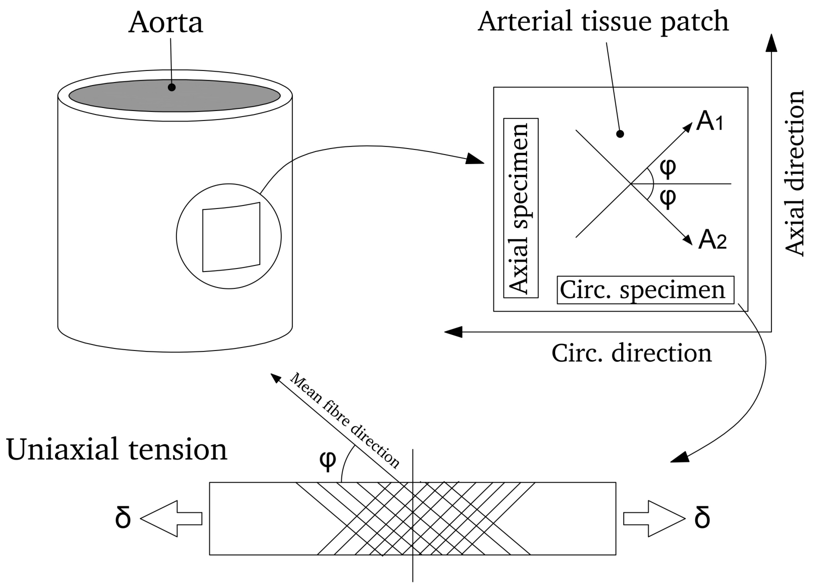

Figure 1. Definition of axial and circumferential specimens and uniaxial tension test configuration (adapted from Gasser et al. (2006)). A_1 and A_2 represent the mean direction of each family of fibers.

Table 1. Constitutive parameters for the layer-separated specimens and the intact (three-layer composite) wall of the human abdominal aorta (taken from Weisbecker et al. (2012)).

Layer	μ(MPa)	k_1(MPa)	$k_2(-)$	$\varphi(^\circ)$	$\kappa(-)$
Intima	0.044	10.14	0.00	40.5	0.25
Media	0.028	0.81	12.42	39.1	0.18
Adventitia	0.010	0.38	3.35	40.59	0.11
Intact wall	0.019	5.15	8.64	38.8	0.24

fact that, the bulk modulus of an incompressible material is much greater than its shear modulus. Due to this, a displacement-based element is not suitable since a pure hydrostatic stress state would not produce changes in the displacement field. Therefore, a mixed formulation, using not only displacement but stress variables, is required to solve the equilibrium equations. For that purpose, hybrid elements are used in our simulations to model the incompressible behavior of soft tissue, which is a realisitc assumption since it is mostly made up of water. Values of the Cauchy stresses and strains were computed for each integration point in the tensile direction. The results are compared in terms of stress vs strain curves with the experimental results obtained by Weisbecker et al. (2012).

3.1. FEM analysis results for the uniaxial tests of aorta strips

Figure 2 shows the computed Cauchy stress in the tensile direction for the circumferential and axial three-layered patches at a total displacement of 2.5 mm. In agreement with the results obtained by Gasser et al. in (Gasser et al. 2006) no significant change is observed in the thickness of the specimens, while the width decreases in the middle part of the strips due to the incompressibility constraint. Despite the similarity of the transition zones at the end of strips, all the specimens show a stiffer response in the circumferential direction. Tunica intima exhibits the maximum stress values of the layer-separated specimens, reaching stresses of 2.5 MPa when it is cut in the circumferential direction. The adventitial and medial strip, with maximum values of 1 and 1.2 MPa respectively, present a softer behavior than the intimal strip. One of the main reasons for this is the degree of dispersion of the collagen fibers, κ, which is much higher in the intima ($\kappa = 0.25$) than in any other layer. κ controls the start of the stiffening effect produced by the alignment of the collagen fibers in the direction of the applied load, therefore, higher values of κ provide a stiffer response at equal streches. Concerning the intact and the three-layered patch, we observe a parallel structural response for the first one compared to the above analyzed separated intima layer: the high dispersion of the collagen fibers for this case, $\kappa = 0.24$, which is in fact very similar to the value of the intima layer, $\kappa = 0.25$, leads to a macroscopic stiffer behaviour, where fibers do not need to rotate before carrying load and just a small reduction of the width of the specimen is noticed. On the other hand, the three-layered patch shows a dissimilar mechanical behaviour in which we observe noteworthy stress discontinuities between the layers where the intima is absorbing the largest amount of stress.

Figure 3 shows the stress versus stretch response in the direction of the applied load for the circumferential and axial specimens. The Cauchy stress was computed as $\sigma = F\lambda/(TW)$, where F stands for the applied force, T for the thickness of the specimen, W for the width (both in the undeformed configuration), and $\lambda = l/L$ represents the stretch in the loading direction, where l and L are the lengths of the specimen in the deformed and reference configuration, respectively. The qualitative stress-stretch response of the three-layered patch is similar to the one reported by Holzapfel et al. (2005) for coronary arteries, and Weisbecker et al. (2012) for the abdominal aorta. As it can be seen, the intima manifests an early exponential stiffening at low stretches in both circumferential and axial directions. This stress-stretch response is closely related to the high degree of dispersion in the collagen fiber directions previously commented, which is in turn, associated with the collagenization of the innermost hyperelastic layer during the development of the diffuse intimal thickening of the aorta (Movat et al. 1958). Media and adventitia curves show a softer behavior in both directions, where the exponential stiffening produced by the anisotropic contribution of the collagen fibers to the strain energy function is delayed in comparison to the intimal layer. For a total Cauchy stress of 0.7 MPa, the axial specimen of the intimal layer reachs a maximum stretch of 1.24, while adventitial and medial strips have maximum streches of 2.5 and 1.5, respectively. As for the three-layered tissue, despite being made up of intima, media and adventitia, its mechanical reaction is somewhat less stiff in comparison with the intima and the intact wall, probably due to the loss of strain energy produced during the discontinuous stress migration from tunica intima to the other two layers.

4. Human aorta plane strain rings

Before assessing the effects of the intimal thickening in an AAA geometry, a simpler case is studied. To test the feasibility of the three-layered model proposed, a human aorta plane geometry was modeled with the configuration shown in figure 4. The dimensions of the rings were 10 mm for inner radius and a different thickness depending on the layer modeled. For the layer-separated rings the thickness of each layer is the same as the ones used previously for the uniaxial test simulations: 0.68, 0.94 and 1.07 mm for intima, media and adventitia, respectively. Plane strain boundary conditions were applied for all the models.

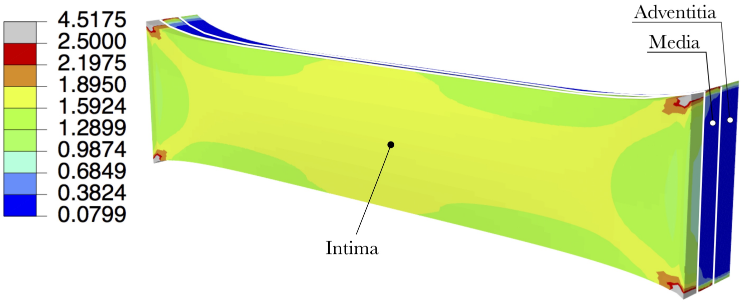

(a) Three-layered patch cut in the circumferential direction.

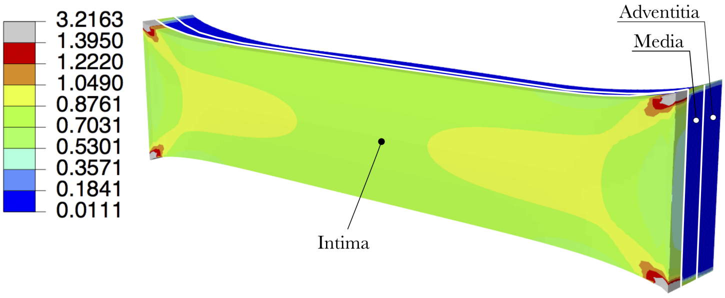

(b) Three-layered patch cut in the axial direction.

Figure 2. Finite element computations of the Cauchy stress in the tensile direction at a displacement of 2.5 mm (MPa). The grey zones are a result of edge effects caused by the stress concentrations due to the displacement constraint applied on the lateral face of the specimen.

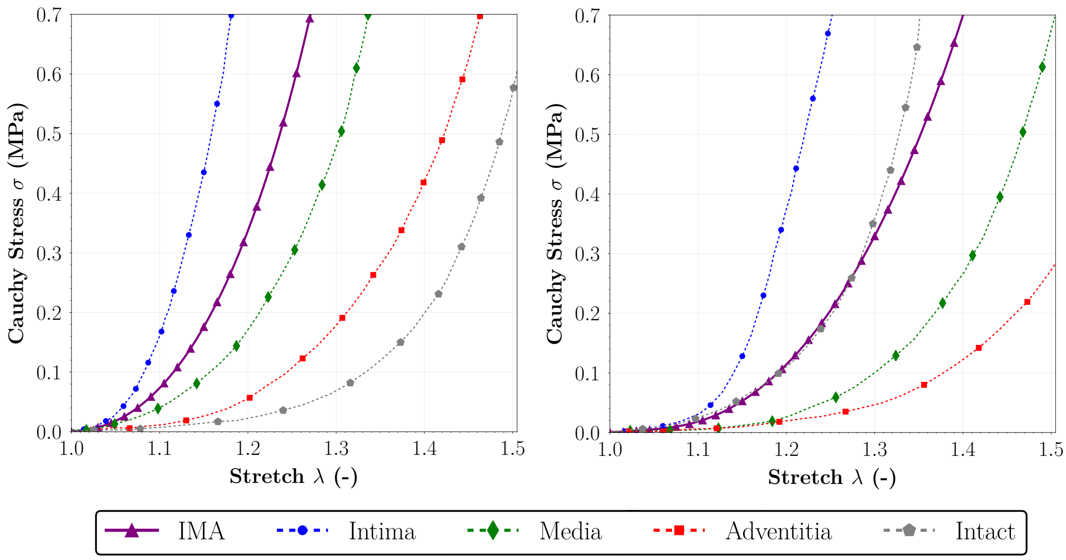

Figure 3. Computed Cauchy stress vs stretch curves of the circumferential (left) and axial specimens (right) in solid purple curve for the IMA (intima-media-adventitia) three-layered tissue patch and the intact tissue patch. Experimental results by Weisbecker et al. (2012) in dashed curves for intima, media and adventitia tissues.

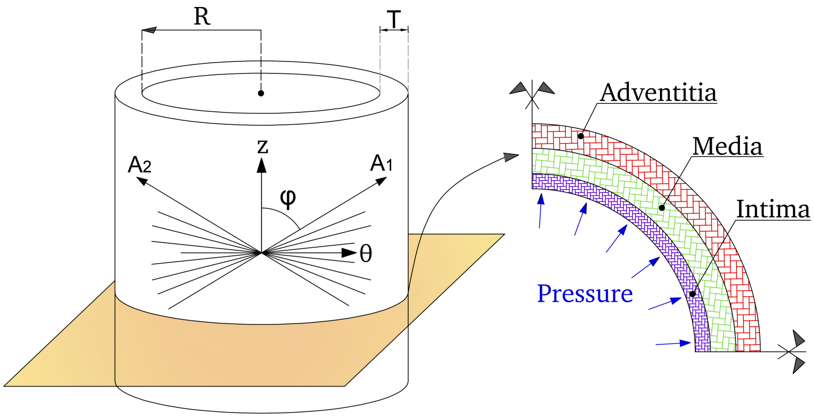

Figure 4. Scheme of the model configuration for the human aorta plane strain rings (adapted from Gasser et al. (2006)).

In order to simulate the end-systolic state, in which the artery undergoes the largest wall stresses, an internal pressure of 16 kPa (120 mmHg) was implemented. Material constants for the layer-separated and intact three-layer composite artery wall are collected in Table 1. Regarding the layer-separated models, 1,215 eight-node solid hybrid elements (C3D8H) were used for intima, 486 elements for the media and 748 elements for the adventitia, with a minimum of two elements through-the-thickness of each layer. In the intact aorta rings a total of 2500 elements were required to obtain precise through-thickness stress distributions. Circumferential stresses and stretches were computed at each integration point across the thickness of the artery wall.

4.1. Results for aorta plane strain rings

The computed circumferential stresses produced by an internal pressure of 16 kPa (120 mmHg) are depicted in Figure 5. The absence of residual stresses leads to a pure tension state through the whole thickness in both the layer-separated and three-layered configurations. Regarding the layer-separated rings, we observe maximal values at the inner radius of the adventitial ring of about 0.32 MPa, which decrease to 0.24 MPa at the outer, while the stress distributions of the media and intima are quite similar at the inner radius, reaching values close to 0.32 MPa, but differ from the outer radius, where the intima shows slightly higher circumferential stresses that go up to 0.28 MPa. Furthermore, we notice big differences between the through-the-thickness circumferential stresses of the intact artery, the two-layered and the three-layered rings, which are depicted in Figure 6. As it can be seen, the intact artery shows an analogous non-linear stress distribution to the one observed previously for the layer-separated cylinders, with a range of stress values that goes from 0.017 MPa at the inner surface to 0.012 at the outer. On the other hand, in agreement with Alastrué et al. (2007), we observe again "the discontinuities caused by the heterogeneity of the two-layered and the three-layered wall". As shown in Figure 6, the existing stress value of 0.224 MPa at the inner part of the intima suddenly drops at the interface with the media, where it took a value of 0.04 MPa. In the same way, another stress jump is found at the interface between media and adventitia, but this time not as important as the previous one, dropping from 0.04 to 0.02 MPa.

The results in terms of internal pressure versus circumferential stretch (p_i/λ_θ) are

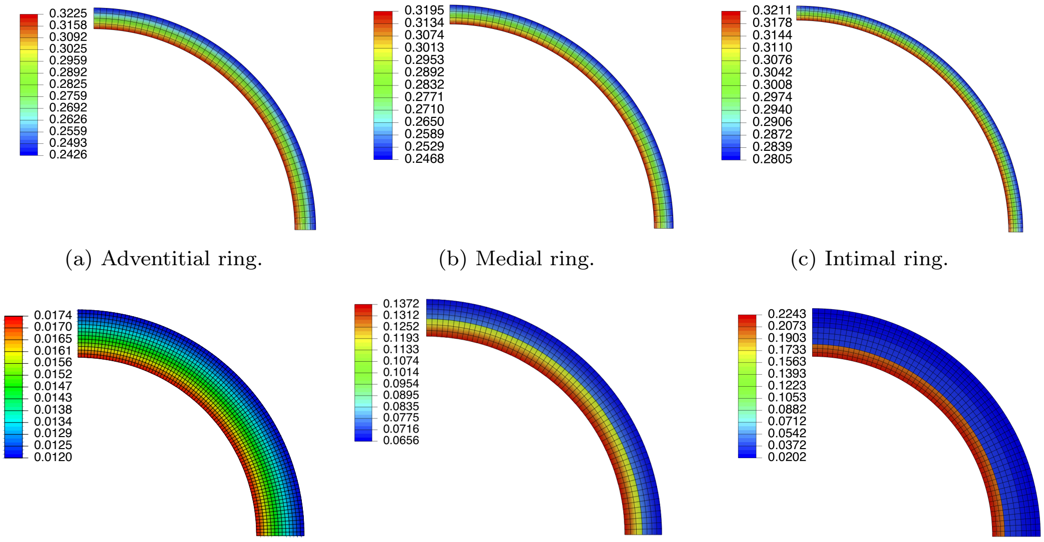

(a) Adventitial ring. (b) Medial ring. (c) Intimal ring.

(d) Intact aorta ring. (e) Two-layered aorta ring. (f) Three-layered aorta ring.

Figure 5. Circumferential stress distributions in the aorta plane strain rings at an internal pressure of 16 kPa. The magnitude of the stresses is given in MPa.

illustrated in Figure 7. Once more we can see how the internal pressure/circumferential stretch response tends to stiffen with increasing κ. As we saw in the uniaxial tests, with an early exponential stiffening, tunica intima is acting again as the stiffest layer, giving a total circumferential stretch of 1.11 at an internal pressure of 16 kPa, while the adventital layer is the softest with a final stretch of 1.34 for the same internal pressure. The medial layer shows a delayed structural response that is between the intima and the adventitia, reaching stretch values of 1.25. The three-layered and the intact rings have a similar pressure/stretch behavior, even if the former one is much stiffer despite the large stress discontinuities at the interfaces between the layers which produce a decrease of the stored strain energy in the collagen fibers.

5. Parametrized idealized geometrical models of AAAs

Once the effects of intimal thickening have been assessed in simpler geometries, a more realistic shape is needed to take into account the influence of the typical geometrical non-linearity that characterises fusiform aneurysms, which are the most common ones. For this purpose, an in-house code (Díaz 2016) was developed. This code uses the application program interface of the open source CAD/CAE package SALOME (201 2015) to create the digital model of three-dimensional extruded solid geometries. The code considers all the geometric and physical variables that characterise an idealized aneurysm, such as length, azymuthal asymmetry, wall thickness, the undilated diameter at the inlet/outlet sections and the maximum diameter at the midsection of the AAA. The circular cross sections have the ability to rotate around the three axis, and the geometries are different in terms of wall heterogeneity and asymmetry, which are depicted by cross sections perpendicular to the z-axis, hence coinciding with its centerline. The asymmetry is given by β and is defined as $\beta = r/R$ and schematically illustrated in Figure 8 as originally proposed by Vorp et al. (1998), where r and R are the radius measured at the midsection of the AAA cavity from the longitudinal

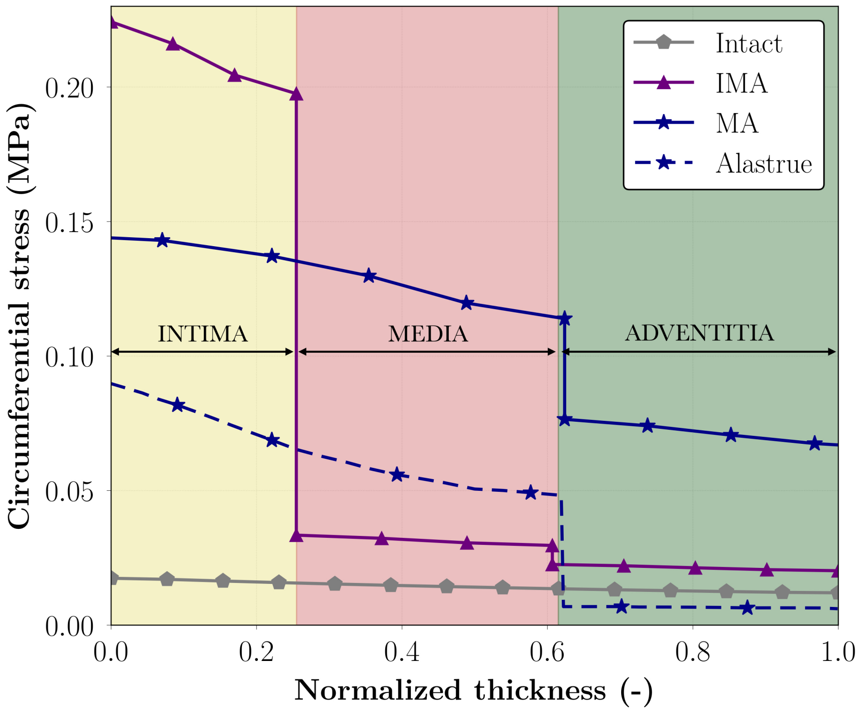

Figure 6. Through-the-thickness circumferential stresses of the three-layered (IMA), two-layered (MA) and intact artery rings. Comparison with the results obtained by Alastrué et al. (2007) for a two-layered human iliac artery plane strain ring when an internal pressure of 16 kPa is applied without residual stresses (MPa).

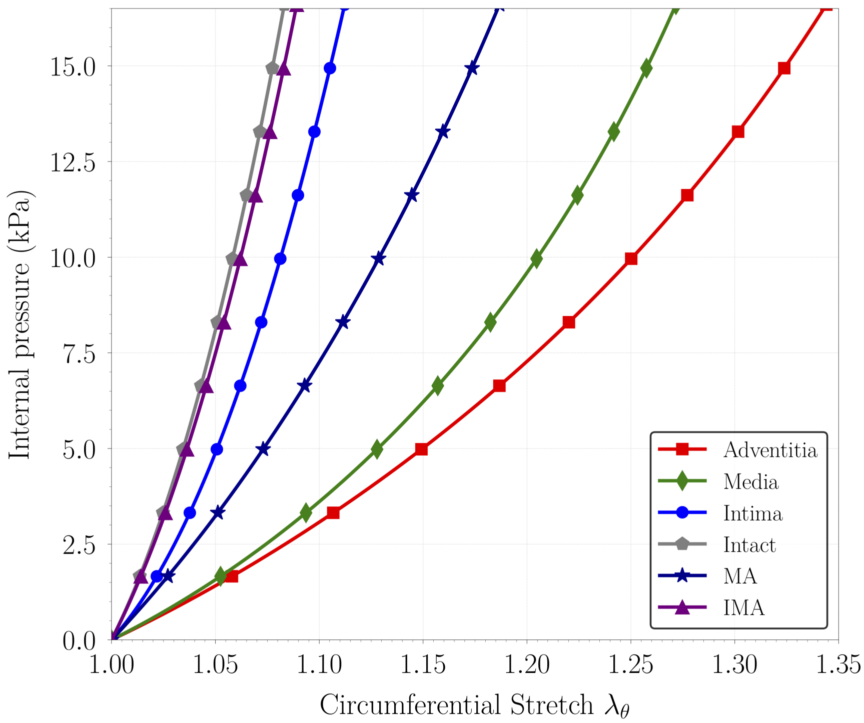

Figure 7. Computed internal pressure versus circumferential stretch of the aorta rings at an internal pressure of 16 kPa.

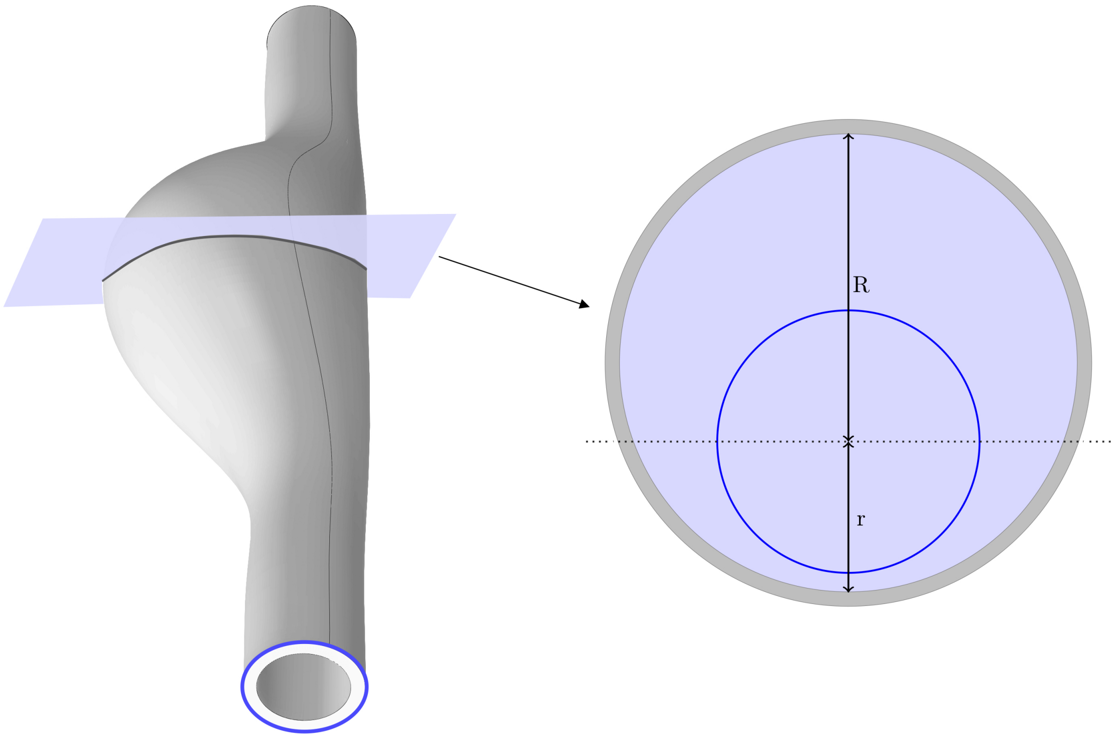

Figure 8. Graphical description of the azymuthal asymmetry.

z-axis to the posterior and anterior walls, respectively. An aneurysm for which only the anterior wall is dilated whereas the posterior wall is approximately flat, corresponds to a value of $\beta = 0.2$. A value of $\beta = 1.0$ corresponds to azymuthal symmetry.

Following the aforementioned procedure, three different geometries of AAA models with a total length of 23 cm were generated, varying the value of the asymmetry parameter between $\beta = 1.0$ (azymuthal symmetry) and $\beta = 0.2$ (only the anterior wall is dilated), with a medium value of $\beta = 0.6$. A value of $d = 2$ cm was adopted for the undilated diameter at the inlet and outlet sections, and a maximum diameter of 6 cm was considered at the midsection of the AAA sac. The common value used from a clinical outlook to recommend surgical repair or endovascular intervention is AAA transverse diameter between 5 and 6 cm (Galland et al. 1998). Consequently, a maximum diameter of 6 cm was chosen for this study, since it is comparable to the largest transverse dimension for assessment of rupture potential. Considering that this is not a patient-specific study, the uniform wall thickness assumption seems to be reasonable. In this manner, a total constant wall thickness of 2.69 mm has been adopted in all the geometries. For the layer-separated models, the thicknesses for intima, media and adventitia remain the same as the ones considered previously (0.68, 0.94 and 1.07 mm). The resultant geometries are depicted in Figure 9.

The effect of the luminal pressure at the end-systolic state was simulated once again by applying an internal static pressure of 16 kPa (120 mmHg) on the inner surface of the aneurysm. We do not use a dynamic loading since no change can be observed for the hyperelastic model with respect to simple static loading, if neither viscoelastic model nor Fluid Structure Interaction analysis is considered. Residual stresses have been generally neglected in this study. These simplification is typically used when dealing

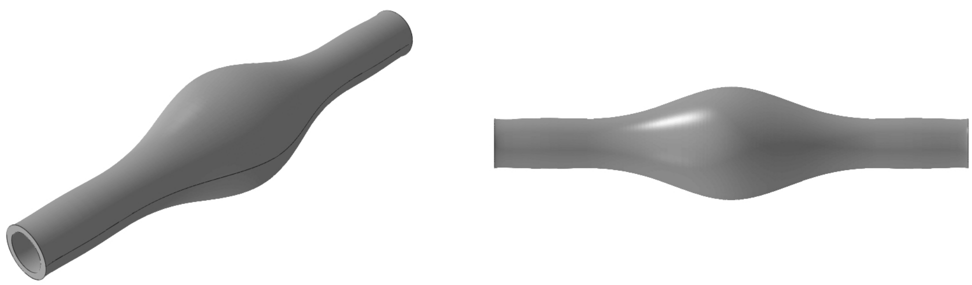

(a) $\beta = 1.0$.

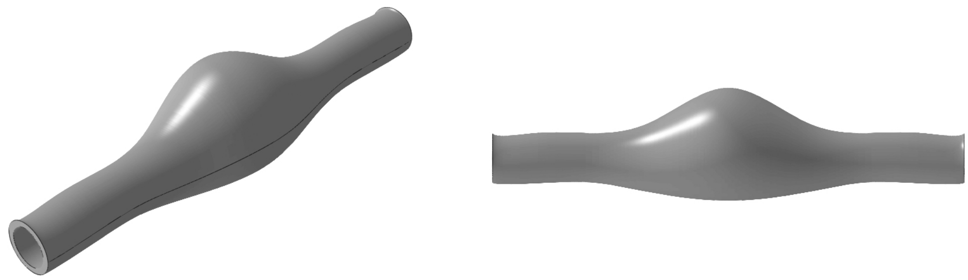

(b) $\beta = 0.6$.

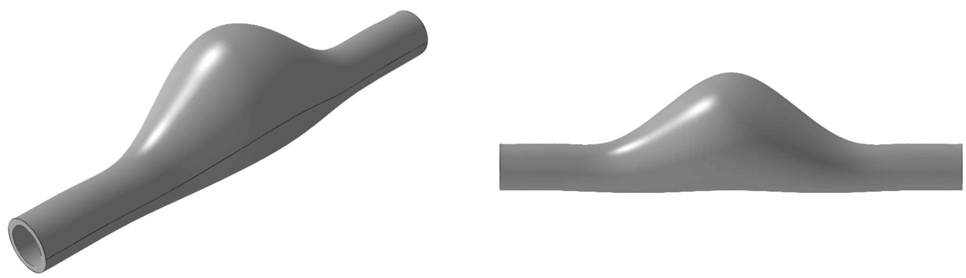

(c) $\beta = 0.2$.

Figure 9. Idealized geometries of the AAA models considered in the study.

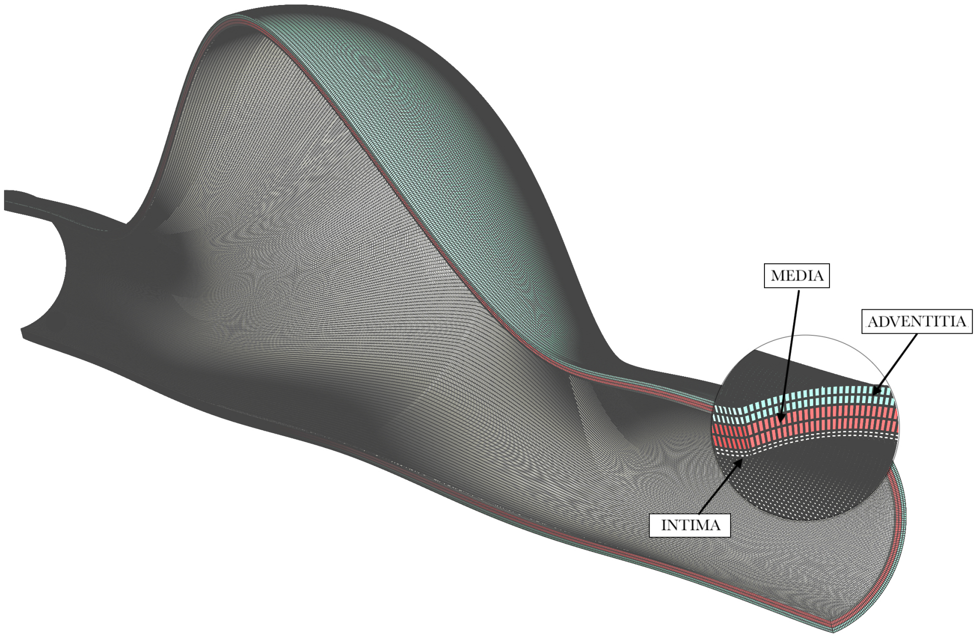

Figure 10. Sagittal view of the typical mesh used for the simulations of the three-layered aneurysms. This geometry corresponds to $\beta = 0.2$.

with complicated 3D AAA geometries (Li et al. 2010; Gee et al. 2010; Humphrey and Holzapfel 2012; Strbac et al. 2017). In our case, given that we are considering a multilayered wall, it would be even more complicated to quantify the value of the residual stresses for each layer. Therefore, the implementation of residual stresses is out of the scope of this paper and it will be prepared for a forthcoming publication. Nevertheless, our study is relevant in elucidating the limits and uncertainties introduced by this assumption.

Applying proper boundary conditions referred to a cylindrical coordinate system, the constraining effect caused by the iliac and renal arteries was simulated by imposing zero longitudinal displacement at both ends of the undilated sections (Vorp et al. 1998). Even though this type of boundary conditions smooths the numerical response (Rodríguez et al. 2008), the length of the AAA must be enough not to produce stiffening effects along the geometry and stress concentrations at the proximal and distal parts. The three-dimensional AAA geometries were meshed using *ABAQUS/CAE* preprocessor with a minimum of two linear solid hexaedral hybrid elements (C3D8H) across the thickness of each layer, so detailed results in terms of peak wall stresses can be obtained. The element sizes were the same as the ones used previously for the plane strain aorta rings and the uniaxial specimens, but extended into the third dimension maintaining a proper aspect ratio. Figure 10 shows an example of the typical mesh used for the simulations. Table 2 shows a quantitative summary of the meshes with the total number of elements and nodes used for each AAA model.

5.1. Results for the idealized aneurysm models

Distributions of the circumferential stresses, as well as displacement fields in end-systolic conditions for three different values of β are depicted in Figure 11 and Figure 13, respectively (only one-half of the geometry cut by a sagittal plane is shown for clarity).

Table 2. Number of elements and nodes used in the three different parametrized geometrical models of AAAs studied.

AAA model	Number of elements		Number of nodes	
	Three-layered	Intact	Three-layered	Intact
$\beta = 1.0$	$514,080$	$466,480$	$1,091,910$	$1,005,040$
$\beta = 0.6$	$481,500$	$440,608$	$1,017,288$	$949,560$
$\beta = 0.2$	$649,000$	$548,544$	$1,370,611$	$1,202,011$

First of all, it is important to mention that we have taken the circumferential stress as the prevailing stress, since the maximum principal stresses are almost perfectly aligned with the circumferential direction. This is in agreement with some data on aneurysms that identify normal stresses as a more reliable indicator than Von Mises stress, a yield criterion developed for ductile metals which is not a suitable measure in this case because of the absence of shear stress (Raghavan et al. 2006, 2011). As it can be seen in Figure 11, both the intact and the three-layered artery present a stress gradient through-the-thickness of the aneurysmal wall, in which the inner surface absorbs the maximum circumferential stresses. As shown in Figure 12, this through-the-thickness stress variation is fairly flat for the intact artery, with maximum stress differences that go from 0.20 to 0.23 MPa in the $\beta = 0.2$ geometrical model. However, as previously noticed in the plane strain rings, the three-layered AAA models show a remarkable discontinuous gradient that is manifested in huge stress jumps at the interface between the layers, where the major stress drop is found at the interface between the intima and the media in all the models, with a maximum value of 0.64 MPa in the most asymmetric aneurysm ($\beta = 0.2$).

That said, and in good agreement with Rodríguez et al. (2008), it is worth pointing out that the degree of asymmetry is rather considerable: for aneurysms with the same length, wall thickness and diameter of the undilated sections, the peak wall stresses increase by 32% from the symmetric ($\beta = 1.0$) to the most asymmetric geometry ($\beta = 0.2$). Thus, we can say that the geometry, and more specifically the asymmetry of the sac is a determining factor to rupture potential since the strongest stress gradients are always located at inflection points of the curvature. For $\beta = 1.0$ the maximum stress is distributed uniformly around the sac, as well as the highest displacements are, which is logical due to the azymuthal symmetry. In case of the $\beta = 0.6$ and $\beta = 0.2$ geometries, notable stress concentrations occur for both the three-layered and the intact wall at the superolateral part of the sac. By contrast, the maximum displacements are found in the inferior part, which is fairly flat. This phenomena responds to the principles of the membrane theory of shells: because the artery wall can be considered as a structural element with a small thickness compared to the other dimensions, we can say that the stiffening at the inflection points is due to the combination between membrane and bending forces produced by the curvature, while the flatness of the inferior part only generates bending forces which leads to a softer response with larger displacements. Table 3 summarises the peak wall stresses obtained for each model and establish a comparison, in terms of stresses and displacements, between the three-layered and the intact models with respect to the former one. Regarding the peak stress values, we observe an overall stress difference of about 30% that slightly increases with asymmetry, reaching a maximum $\Delta\sigma_{\max}$ of 35.9% for the $\beta = 0.2$ aneurysm. Contrastingly, variations in displacements decrease with the asymmetry from a noteworthy $\Delta \mathrm{U}_{\max}$ about 54% for $\beta = 1.0$ to a insignificant difference of 0.75 % for the $\beta = 0.2$ geometry.

To assess the effects of the heterogeneity of the aneurysmatic wall and the material anisotropy, we have compared our results for the hyperelastic three-layered anisotropic (H3A) AAA wall with the results obtained by Scotti et al. (2005, 2008), where also peak wall stresses and displacements are analyzed in parametrized aneurysms. We have chosen this study to establish a comparison, given that the parameterization of the AAA geometries is the same, considering $\beta = r/R$ to define the asymmetry of sac, and a similar systolic pressure of 15.7 kPa (118 mmHg). Comparisons are made between our H3A wall, in which each layer work independently, a elastic isotropic mono-layered (EIM) and a hyperelastic isotropic mono-layered wall (HIM), based on the Mooney-Rivlin constitutive model. The results of the comparison are collected in Table 4. In terms of stresses, first of all we observe how the percentage difference increases with the asymmetry: for the elastic wall (EIM) the range of difference is between 43% and 54%, while for the HIM, given that the hyperelastic wall can undergo larger deformations than the elastic one, and therefore develops higher stresses, the differences are between 38% and 51%, both maximum differences associated with the most asymmetric AAA ($\beta = 0.2$). Regarding the displacements, for the EIM wall the differences become greater as the asymmetry increases, reaching a maximum variation of 48%. Strikingly, for asymmetry values of $\beta = 1.0$ and $\beta = 0.6$ the HIM wall undergo larger deformations than the H3A wall, with a maximum difference of 9.43%, probably due to the stiffening effect produced by tunica intima in the inner surface of the artery. The displacements of the most asymmetric AAA geometries, $\beta = 0.2$, are quite similar with a small variation of just 0.75%.

One of the main advantages of the layer-separated models is that we can easily isolate the layers to see the maximum stresses of each one. The circumferential stress distributions of adventitia, media and intima during systole are depicted in Figure 14 for the three different AAA models. As it can be seen, the patterns of circumferential stresses remain unchanged from the anterior to the posterior wall of the AAA in all cases, with a uniform distribution around the sac for the symmetric model, and stress concentrations at the inflection points of the curvature of the sac in the asymmetric aneurysms as previously commented, which means that, despite the significant stress jumps found in Figure 12, there is a strong stress transmission from the inner to the outer wall of the sac that is damped by the tunica intima, which acts as a natural stiffener for the artery. Table 5 summarizes the percentage of stress absorbed by each layer with respect to the total circumferential stress. This percentage is measured by what we have called mean stress absorption. As shown, the intima is the stiffest layer, absorbing a minimum of 0.443 MPa and maximum of 0.645 MPa during peak systolic, which leads to stress absorptions of 80.49% and 80.42% for the $\beta = 1.0$ and $\beta = 0.2$ respectively and a mean absorption of 78.33%. The adventitia is the softest layer, with a range of values between 0.193 and 0.251 MPa, and a mean stress absorption of 7.68%, while the media is a bit stiffer with a 11.05%. These results are in accordance with the previously analyzed uniaxially loaded aorta strips and the inflated plane strain rings, where the early stiffening effect of the intima due to the high dispersion of the collagen fibers was predicted.

The computed circumferential stresses in our idealized AAAs are similar to the circumferential Cauchy failure stresses reported by Sassani et al. (2015): 0.51 MPa for the intima, 1.09 MPa for the media and 1.73 MPa for the adventitia. According to these failure stress values, we can conclude that the intima layer ruptures for asymmetry values of $\beta = 0.6$ and $\beta = 0.2$. It is only in the case of azimuthal symmetry, with $\beta = 1.0$, that the intima withstands the load exerted by the luminal pressure. This conclusion is consistent with two statements that reinforce the importance of including the intima in multi-layered models of AAAs: the rupture begins in the intima; and the

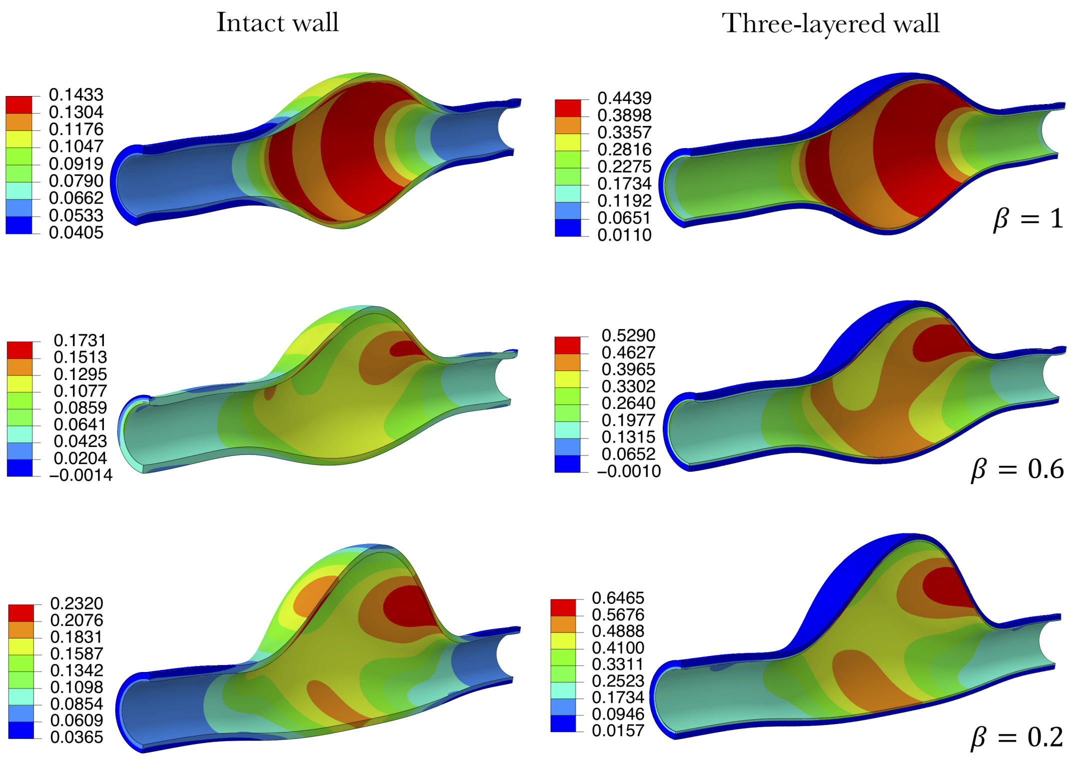

Figure 11. Contour plots of the circumferential stresses in the intact and in the three-layered aneurysmatic wall for asymmetry values of $\beta = 1.0$, $\beta = 0.6$ and $\beta = 0.2$ during peak systolic (MPa).

asymmetry of the sac increases the probability of aneurysm rupture. Even though the peak wall stresses will be smoothed if we include residual stresses, the results obtained by our idealized AAAS are accurate enough.

6. Conclusions

This investigation attempts to demonstrate the importance of considering the mechanical contribution of the three layers that make up aortic tissue during the development of intimal hyperplasia. To do this, finite element analyses were performed on three different idealized geometries of AAA models subjected to realistic loading and boundary conditions. These simulations were calibrated considering the structural response of the aneurysmal tissue through uniaxial tests of aorta strips cut in the circumferential

Table 3. Maximum circumferential wall stresses $\sigma_{\max}$ and displacements $U_{\max}$ in the different asymmetric AAA models and comparison between the three-layered and the intact artery wall. $\Delta\sigma_{\max}$ and $\Delta\mathrm{U}_{\max}$ show the % difference of the stress and displacement obtained with the three-layered and intact AAA models with respect to the baseline three-layered method.

AAA model	$\sigma_{\max}$ (MPa)		$\mathrm{U}_{\max}$ (mm)		$\Delta\sigma_{\max}$%	$\Delta\mathrm{U}_{\max}$%
	Three-layered	Intact	Three-layered	Intact		
$\beta = 1.0$	0.44	0.14	2.65	1.22	31.8	53.96
$\beta = 0.6$	0.52	0.17	3.76	3.24	32.7	13.82
$\beta = 0.2$	0.64	0.23	6.65	6.60	35.9	0.75

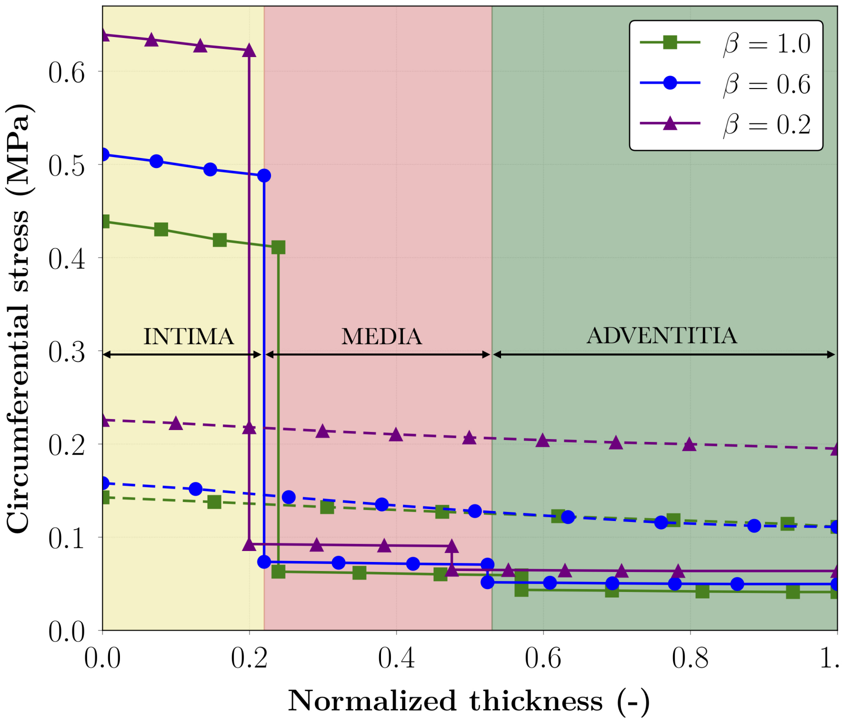

Figure 12. Through-the-thickness circumferential stresses in the three-layered (solid curves) and intact (dashed curves) AAA wall for asymmetry values of $\beta = 1.0$, $\beta = 0.6$ and $\beta = 0.2$.

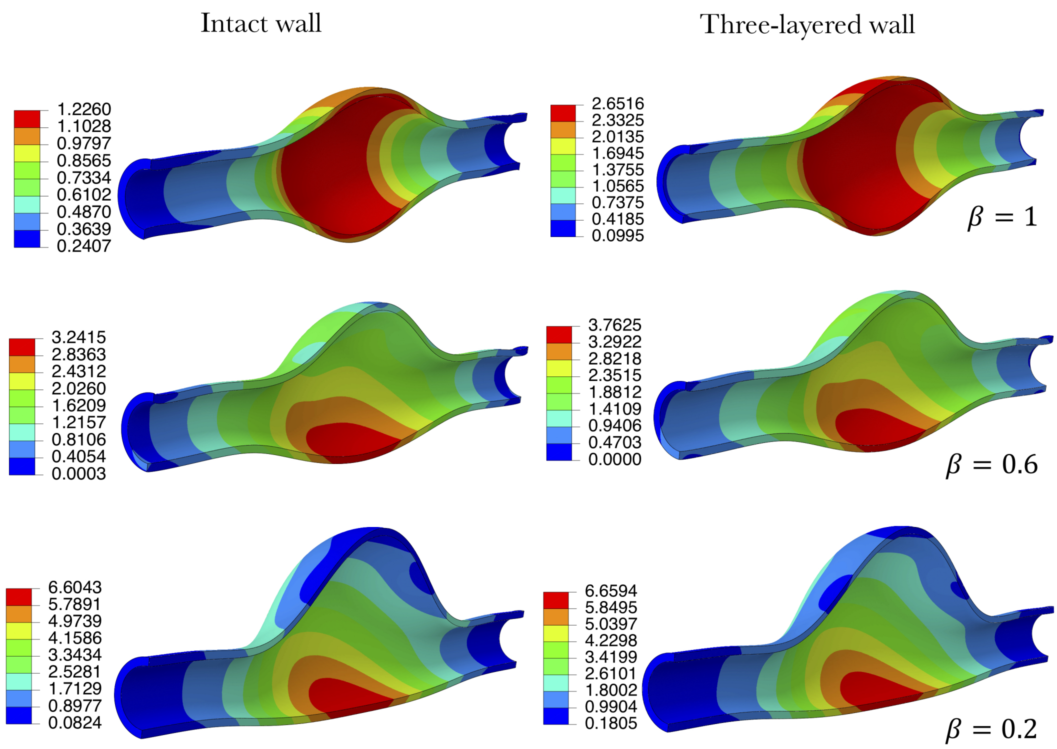

Figure 13. Displacement fields in the intact and in the three-layered aneurysmal wall for asymmetry values of $\beta = 1.0$, $\beta = 0.6$ and $\beta = 0.2$ during peak systolic, in mm.

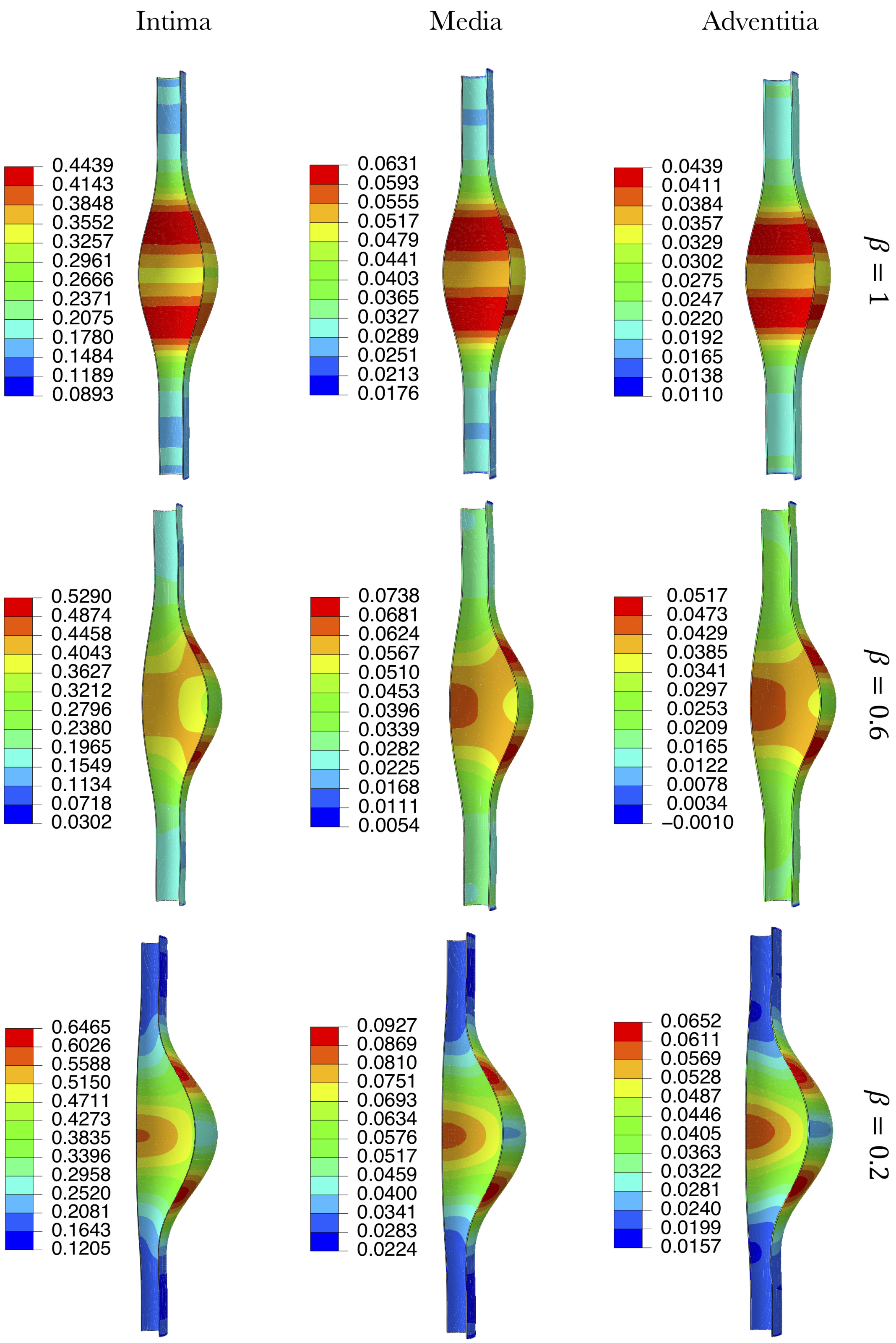

Figure 14. Circumferential stress distributions in adventitia, media and intima layers for $\beta = 1.0$, $\beta = 0.6$ and $\beta = 0.2$ models. The magnitude of the stress is given in MPa.

Table 4. Maximum wall stresses $\sigma_{\max}$ and displacements $U_{\max}$ in the different asymmetric hyperelastic anisotropic three-layered (H3A) AAA models at a peak systolic pressure of 16 kPa (120 mmHg) and comparison with the results obtained by Scotti et al. (2005, 2008) for the same geometries and a similar systolic blood pressure of 15.7 kPa for an elastic isotropic mono-layer (EIM) and a hyperelastic isotropic (Mooney-Rivlin) mono-layer AAA wall. The parenthesis show the % differences of the EIM and the HIM with respect to the H3A.

AAA model	$\sigma_{\max}$ (MPa)			$U_{\max}$ (mm)		
	EIM	HIM	H3A	EIM	HIM	H3A
$\beta = 1.0$	0.25(−43.18%)	0.27(−38.63%)	0.44	1.71(−35.47%)	2.90(+9.43%)	2.65
$\beta = 0.6$	0.26(−50.00%)	0.28(−46.15%)	0.52	2.50(−33.51%)	4.30(+14.36%)	3.76
$\beta = 0.2$	0.29(−54.68%)	0.31(−51.56%)	0.64	3.40(−48.87%)	6.60(−0.75%)	6.65

Table 5. Maximum circumferential wall stresses (MPa) in adventitia, media and intima and mean percentage of peak wall stress absorbed by each layer for the three different AAA models. The parenthesis show the percentage of stress absorbed by each layer with respect to the total circumferential stress.

AAA model	$\sigma_{\max}$ (MPa)		
	Adventitia	Media	Intima
$\beta = 1.0$	0.043(7.83%)	0.063(11.49%)	0.443(80.69%)
$\beta = 0.6$	0.051(7.12%)	0.073(10.19%)	0.529(73.88%)
$\beta = 0.2$	0.065(8.10%)	0.092(11.47%)	0.645(80.42%)
Mean stress absorption	7.68%	11.05%	78.33%

and axial directions and plane strain human aorta rings under systolic blood pressure.

Resultant stresses and displacements were obtained for an intact (mono-layered) artery wall, which represents the adventitia-intima-media in a single layer with averaged properties, and a three-layered wall, in which each layer has been modeled separately with its own material properties using a continuum mesh. We observed differences of about 30% concerning the stresses and a maximum of 53% in displacements. This comparison was also carried out with other studies performed on idealized AAA geometries with the same parameterization, but with different constitutive models. We found out maximum differences of 54% in terms of stresses and 48% in terms of displacements for an elastic isotropic mono-layered wall (EIM), and 51% and 14% for a hyperelastic isotropic mono-layer wall (HIM), with respect to a three-layered hyperelastic anisotropic wall (H3A).

Regarding the idealized geometries used, our results corroborate that the stress distribution is strongly dependent on the asymmetry of the sac. Symmetric AAAs showed a uniform stress distribution around the sac, while the most asymmetric geometries presented noteworthy stress concentrations at the inflection points of the curvature of the sac, leading to greater peak wall stresses, and therefore higher rupture potential.

The obtained results show an early exponential stiffening of tunica intima that makes it definitely load-bearing when it becomes thickened because of intimal hyperplasia. Intimal hyperplasia may be caused by two factors. The first one is the collagenization; The diffuse thickening of the innermost layer of the abdominal aorta has been associated by many studies with collagenization of the elastic and hyper-plastic layers, which increases the dispersion in the families of collagen fibers and stiffens up the intimal layer. The second factor could be related to the proliferation of smooth muscle cells between the endothelium and the internal elastic lamina. In any case, the intimal layer shows the highest percentages of stress absorption.

Our results suggest that tunica intima acts as a stiffener when thickened due to hyperplasia. The intima shows a mean stress absorption ratio of 78%, while the adventitial and medial layers only absorb 7% and 11% of the total circumferential stress on the AAA, respectively. The peak wall stresses in the three-layered AAA models are comparable to the experimental results obtained by Kobielarz et al. (2017) for young arteries in the initial stages of atherosclerotic process, and the investigations carried out by Akyildiz et al. (2014) for human atherosclerotic intima tissue. These facts point out the necessity of including tunica intima in multi-layered models of AAAs to obtain accurate peak wall stresses, and to improve the rupture risk assessment.

The models developed in this investigation have three important limitations. First, the material properties are obtained from non-aneurysmal aortas and then applied to idealized AAA geometries. Second, the constitutive model used only considers two families of collagen fibers. And last but not least, residual stresses are not included.

The first two limitations will be bypassed in forthcoming publications by considering the mechanical properties of aneurysmal abdominal aortas as in (Kobielarz et al. 2017), and by incorporating a third family of collagen fibers as in (Sassani et al. 2015). Even though these two new assumptions will make our models more precise in predicting the risk of rupture, we do not expect substantial changes in the overall mechanical response of the multilayered wall.

If residual stresses are included, we expect a decrease in the compressive stresses in the intima and the tensile stresses in the media and adventitia. In agreement with Sokolis (2015), residual stresses will lessen the stress jumps at the interface between the intima and the media. Nevertheless, we believe that the thickened intima will remain as the layer with the higher stress absorption ratio.

This research is a first step in the development of a three-layered model to simulate the mechanical behavior of the abdominal aorta in a more precise way. The model should be improved in future works by incorporating residual stresses and layer-specific properties obtained from aneurysmal aortas.

Acknowledgements

The research leading to these results has received funding from the Galician Regional Government (*Xunta de Galicia*) under grant agreement *Grupos de referencia competitiva ED431C 2017/72*. The authors fully acknowledge the support received. Mr. de Lucio also acknowledges the funding received from the Spanish Government (*Ministerio de Educación Cultura y Deporte*) under the programme *Becas de colaboración de estudiantes en departamentos universitarios para el curso académico 2017-2018*.

References

2014a. Abaqus 6.14 benchmarks guide, material tests, anisotropic hyperelastic modeling of arterial layers. Dassault Systèmes.

2014b. Abaqus 6.14 documentation. Dassault Systèmes.

2015. SALOME 7.5.1. The open source integration platform for numerical simulation.

Ahamed T, Dorfmann L, Ogden R. 2016. Modelling of residually stressed materials with application to aaa. Journal of the Mechanical Behavior of Biomedical Materials. 61:221 – 234.

Akyildiz AC, Speelman L, Gijsen FJ. 2014. Mechanical properties of human atherosclerotic intima tissue. Journal of Biomechanics. 47(4):773 – 783. SI: Plaque Mechanics.

Alastrué V, Peña E, Martínez MÁ, Doblaré M. 2007. Assessing the use of the "opening angle method" to enforce residual stresses in patient-specific arteries. Annals of Biomedical Engineering. 35(10):1821–1837.

Amabili M, Balasubramanian P, Bozzo I, Breslavsky ID, Ferrari G. 2019. Layer-specific hyperelastic and viscoelastic characterization of human descending thoracic aortas. Journal of the Mechanical Behavior of Biomedical Materials. 99:27 – 46.

Barrett HE, Van der Heiden K, Farrell E, Gijsen FJ, Akyildiz AC. 2019. Calcifications in atherosclerotic plaques and impact on plaque biomechanics. Journal of Biomechanics. 87:1 – 12.

Chandra S, Raut SS, Jana A, Biederman RW, Doyle M, Muluk SC, Finol EA. 2013. Fluid-structure interaction modeling of abdominal aortic aneurysms: The impact of patient-specific inflow conditions and fluid/solid coupling. Journal of Biomechanical Engineering. 135(8):081001–081001–14.

Deveja RP, Iliopoulos DC, Kritharis EP, Angouras DC, Sfyris D, Papadodima SA, Sokolis DP. 2018. Effect of aneurysm and bicuspid aortic valve on layer-specific ascending aorta mechanics. The Annals of Thoracic Surgery. 106(6):1692–1701.

Díaz J. 2016. Aneupy. A Python code for parametric generation of abdominal aortic aneurysms; [http://github.com/jacobo-diaz/aneupy]; Jun.

Galland R, Whiteley M, Magee T. 1998. The fate of patients undergoing surveillance of small abdominal aortic aneurysms. European Journal of Vascular and Endovascular Surgery. 16(2):104–109.

Gao F, Ohta O, Matsuzawa T. 2008. Fluid-structure interaction in layered aortic arch aneurysm model: assessing the combined influence of arch aneurysm and wall stiffness. Australasian Physics & Engineering Sciences in Medicine. 31(1):32.

Gao F, Ueda H, Gang L, Okada H. 2013. Fluid structure interaction simulation in three-layered aortic aneurysm model under pulsatile flow: Comparison of wrapping and stenting. Journal of Biomechanics. 46(7):1335 – 1342.

Gao F, Watanabe M, Matsuzawa T. 2006. Stress analysis in a layered aortic arch model under pulsatile blood flow. Biomedical engineering online. 5:25–25.

Gasser TC, Gallinetti S, Xing X, Forsell C, Swedenborg J, Roy J. 2012. Spatial orientation of collagen fibers in the abdominal aortic aneurysm's wall and its relation to wall mechanics. Acta Biomaterialia. 8(8):3091 – 3103.

Gasser TC, Ogden RW, Holzapfel GA. 2006. Hyperelastic modelling of arterial layers with distributed collagen fibre orientations. Journal of The Royal Society Interface. 3(6):15–35.

Gee MW, Förster C, W AW. 2010. A computational strategy for prestressing patient-specific biomechanical problems under finite deformation. International Journal for Numerical Methods in Biomedical Engineering. 26(1):52–72.

Geest JPV, Sacks MS, Vorp DA. 2006. The effects of aneurysm on the biaxial mechanical behavior of human abdominal aorta. Journal of Biomechanics. 39(7):1324 – 1334.

Georgakarakos E, Ioannou C, Kamarianakis Y, Papaharilaou Y, Kostas T, Manousaki E, Katsamouris A. 2010. The role of geometric parameters in the prediction of abdominal aortic aneurysm wall stress. European Journal of Vascular and Endovascular Surgery. 39(1):42 – 48.

Gholipour A, Ghayesh MH, Zander A, Mahajan R. 2018. Three-dimensional biomechanics of coronary arteries. International Journal of Engineering Science. 130:93 – 114.

Glagov S, Zarins CK. 1989. Is intimal hyperplasia an adaptive response or a pathologic process? observations on the nature of nonatherosclerotic intimal thickening. Journal of Vascular Surgery. 10(5):571–573.

Grootenboer N, Bosch JL, Hendriks JM, van Sambeek MRHM. 2009. Epidemiology, Aetiology, Risk of Rupture and Treatment of Abdominal Aortic Aneurysms: Does Sex Matter?

Hans SS, Jareunpoon O, Balasubramaniam M, Zelenock GB. 2005. Size and location of thrombus in intact and ruptured abdominal aortic aneurysms. Journal of Vascular Surgery. 41(4):584–588.

Holzapfel GA, Gasser TC, Ogden RW. 2000. A new constitutive framework for arterial wall mechanics and a comparative study of material models. Journal of elasticity and the physical

science of solids. 61(1):1–48.
Holzapfel GA, Sommer G, Gasser CT, Regitnig P. 2005. Determination of layer-specific mechanical properties of human coronary arteries with nonatherosclerotic intimal thickening and related constitutive modeling. American Journal of Physiology-Heart and Circulatory Physiology. 289(5):H2048–H2058.
Humphrey J, Holzapfel G. 2012. Mechanics, mechanobiology, and modeling of human abdominal aorta and aneurysms. Journal of Biomechanics. 45(5):805 – 814. Special Issue on Cardiovascular Solid Mechanics.
Kobielarz MJ, Kozuń MM, Kuzan A, Maksymowicz K, Witkiewicz W, Pezowicz C. 2017. The intima with early atherosclerotic lesions is load-bearing component of human thoracic aorta. Biocybernetics and Biomedical Engineering. 37(1):35–43.
Kühnl A, Erk A, Trenner M, Salvermoser M, Schmid V, Eckstein HH. 2017. Incidence, treatment and mortality in patients with abdominal aortic aneurysms: An analysis of hospital discharge data from 2005–2014. Deutsches Ärzteblatt International. 114(22-23):391–398.
Labrosse MR, Gerson ER, Veinot JP, Beller CJ. 2013. Mechanical characterization of human aortas from pressurization testing and a paradigm shift for circumferential residual stress. Journal of the Mechanical Behavior of Biomedical Materials. 17:44 – 55.
Lederle FA, Wilson SE, Johnson GR, Reinke DB, Littooy FN, Acher CW, Ballard DJ, Messina LM, Gordon IL, Chute EP, et al. 2002. Immediate repair compared with surveillance of small abdominal aortic aneurysms. The New England journal of medicine. 346(19):1437–1444.
LeFevre ML. 2014. Screening for abdominal aortic aneurysm: U.S. Preventive Services Task Force recommendation statement. Ann Intern Med. 161(4):281–290.
Li Z, Kleinstreuer C. 2007. A comparison between different asymmetric abdominal aortic aneurysm morphologies employing computational fluid–structure interaction analysis. European Journal of Mechanics - B/Fluids. 26(5):615 – 631.
Li ZY, Sadat U, U-King-Im J, Tang TY, Bowden DJ, Hayes PD, Gillard JH. 2010. Association between aneurysm shoulder stress and abdominal aortic aneurysm expansion. Circulation. 122(18):1815–1822.
Li ZY, U-King-Im J, Tang TY, Soh E, See TC, Gillard JH. 2008. Impact of calcification and intraluminal thrombus on the computed wall stresses of abdominal aortic aneurysm. Journal of Vascular Surgery. 47(5):928 – 935.
Maier A, Gee MW, Reeps C, Eckstein HH, Wall WA. 2010. Impact of calcifications on patient-specific wall stress analysis of abdominal aortic aneurysms. Biomechanics and Modeling in Mechanobiology. 9(5):511–521.
Martino ED, Guadagni G, Fumero A, Ballerini G, Spirito R, Biglioli P, Redaelli A. 2001. Fluid–structure interaction within realistic three-dimensional models of the aneurysmatic aorta as a guidance to assess the risk of rupture of the aneurysm. Medical Engineering & Physics. 23(9):647 – 655.
Movat HZ, More RH, Haust MD. 1958. The diffuse intimal thickening of the human aorta with aging. The American Journal of Pathology. 34(6):1023–1031.
Pierce DM, Fastl TE, Rodriguez-Vila B, Verbrugghe P, Fourneau I, Maleux G, Herijgers P, Gomez EJ, Holzapfel GA. 2015. A method for incorporating three-dimensional residual stretches/stresses into patient-specific finite element simulations of arteries. Journal of the Mechanical Behavior of Biomedical Materials. 47:147 – 164.
Raghavan M, Vorp DA, Federle MP, Makaroun MS, Webster MW. 2000. Wall stress distribution on three-dimensionally reconstructed models of human abdominal aortic aneurysm. Journal of Vascular Surgery. 31(4):760–769.
Raghavan ML, Hanaoka MM, Kratzberg JA, Higuchi MdL, da Silva ES. 2011. Biomechanical failure properties and microstructural content of ruptured and unruptured abdominal aortic aneurysms. Journal of Biomechanics. 44(13):2501–2507.
Raghavan ML, Kratzberg J, Castro de Tolosa EMM, Hanaoka MM, Walker P, da Silva ES, de Tolosa E. 2006. Regional distribution of wall thickness and failure properties of human abdominal aortic aneurysm. Journal of biomechanics. 39(16):3010–3016.

Raghavan ML, Vorp DA. 2000. Toward a biomechanical tool to evaluate rupture potential of abdominal aortic aneurysm: identification of a finite strain constitutive model and evaluation of its applicability. Journal of Biomechanics. 33(4):475–482.

Raghavan ML, Webster MW, Vorp DA. 1996. Ex vivo biomechanical behavior of abdominal aortic aneurysm: assessment using a new mathematical model. Ann Biomed Eng. 24(5):573–582.

Rodríguez JF, Martufi G, Doblaré M, Finol EA. 2009. The effect of material model formulation in the stress analysis of abdominal aortic aneurysms. Annals of biomedical engineering. 37(11):2218.

Rodríguez JF, Ruiz C, Doblaré M, Holzapfel GA. 2008. Mechanical stresses in abdominal aortic aneurysms: Influence of diameter, asymmetry, and material anisotropy. Journal of Biomechanical Engineering. 130(2):021023.

Sassani SG, Kakisis J, Tsangaris S, Sokolis DP. 2015. Layer-dependent wall properties of abdominal aortic aneurysms: Experimental study and material characterization. Journal of the Mechanical Behavior of Biomedical Materials. 49:141 – 161.

Schriefl AJ, Zeindlinger G, Pierce DM, Regitnig P, Holzapfel GA. 2012. Determination of the layer-specific distributed collagen fibre orientations in human thoracic and abdominal aortas and common iliac arteries. Journal of The Royal Society Interface. 9(71):1275–1286.

Scotti CM, Jimenez J, Muluk SC, Finol EA. 2008. Wall stress and flow dynamics in abdominal aortic aneurysms: finite element analysis vs. fluid–structure interaction. Computer Methods in Biomechanics and Biomedical Engineering. 11(3):301–322.

Scotti CM, Shkolnik AD, Muluk SC, Finol Ea. 2005. Fluid-structure interaction in abdominal aortic aneurysms: effects of asymmetry and wall thickness. BioMedical Engineering Online. 4(1):64.

Simsek FG, Kwon YW. 2015. Investigation of material modeling in fluid-structure interaction analysis of an idealized three-layered abdominal aorta: aneurysm initiation and fully developed aneurysms. Journal of biological physics. 41(2):173–201.

Sokolis DP. 2015. Effects of aneurysm on the directional, regional, and layer distribution of residual strains in ascending thoracic aorta. Journal of the Mechanical Behavior of Biomedical Materials. 46:229 – 243.

Sokolis DP. 2019. Regional distribution of layer-specific circumferential residual deformations and opening angles in the porcine aorta. Journal of Biomechanics. 96:109335.

Sokolis DP, Kritharis EP, Iliopoulos DC. 2012. Effect of layer heterogeneity on the biomechanical properties of ascending thoracic aortic aneurysms. Medical & Biological Engineering & Computing. 50(12):1227–1237.

Sokolis DP, Savva GD, Papadodima SA, Kourkoulis SK. 2017. Regional distribution of circumferential residual strains in the human aorta according to age and gender. Journal of the Mechanical Behavior of Biomedical Materials. 67:87 – 100.

Strbac V, Pierce D, Rodriguez-Vila B, Sloten JV, Famaey N. 2017. Rupture risk in abdominal aortic aneurysms: A realistic assessment of the explicit gpu approach. Journal of Biomechanics. 56:1 – 9.

Vito RP, Hickey J. 1980. The mechanical properties of soft tissues—ii: The elastic response of arterial segments. Journal of Biomechanics. 13(11):951 – 957.

Vorp DA, Raghavan M, Webster MW. 1998. Mechanical wall stress in abdominal aortic aneurysm: Influence of diameter and asymmetry. Journal of Vascular Surgery. 27(4):632–639.

Wang DH, Makaroun MS, Webster MW, Vorp DA. 2002. Effect of intraluminal thrombus on wall stress in patient-specific models of abdominal aortic aneurysm. Journal of Vascular Surgery. 36(3):598 – 604.

Wang X, Li X. 2011. Computational simulation of aortic aneurysm using fsi method: Influence of blood viscosity on aneurismal dynamic behaviors. Computers in Biology and Medicine. 41(9):812 – 821.

Weisbecker H, Pierce DM, Regitnig P, Holzapfel GA. 2012. Layer-specific damage experiments and modeling of human thoracic and abdominal aortas with non-atherosclerotic intimal thickening. Journal of the Mechanical Behavior of Biomedical Materials. 12:93–106.

Xenos M, Rambhia SH, Alemu Y, Einav S, Labropoulos N, Tassiopoulos A, Ricotta JJ, Bluestein D. 2010. Patient-based abdominal aortic aneurysm rupture risk prediction with fluid structure interaction modeling. Annals of Biomedical Engineering. 38(11):3323–3337.